# Description of two-dimensional altermagnetism: Categorization using spin group theory

Sike Zeng and Yu-Jun Zhao*

*Department of Physics, South China University of Technology, Guangzhou 510640, China*

(Received 7 May 2024; revised 25 June 2024; accepted 16 July 2024; published 2 August 2024)

Altermagnetism, recently spotlighted in condensed matter physics, presents captivating physical properties and holds promise for spintronics applications. This study delves into the theoretical description and categorization of two-dimensional altermagnetism using spin group theory. Employing spin-group formalism, we establish seven distinct spin layer groups, extending beyond the conventional five spin Laue groups, to describe two-dimensional altermagnetism. Utilizing these findings, we classify previously reported two-dimensional altermagnets and identify different materials exhibiting altermagnetism. Specifically, monolayer $MnTeMoO_6$ and $VP_2H_8(NO_4)_2$ are predicted to be two-dimensional altermagnets. Furthermore, we scrutinize their spin-momentum-locking characteristics through symmetry analysis and density functional theory calculations, substantiating their altermagnetic properties.

DOI: 10.1103/PhysRevB.110.054406

## I. INTRODUCTION

Altermagnetism, characterized by collinear-compensated magnetic order in real space and time-reversal symmetry breaking in reciprocal space, has recently attracted considerable attention in condensed matter physics [1–4] for its intriguing physical properties and promising application in spintronics. This phenomenon was proposed in scientific literature as early as 2019 [5–9] and subsequently formalized with the name "altermagnetism" in 2022 [10]. In the realm of nonrelativistic spin groups [11–13], altermagnetism has emerged as a distinct third magnetic state, characterized by the connection between opposing sublattices through rotational or mirror symmetries, rather than through translational or inversional symmetries, leading to the disruption of $\mathcal{PT}$ symmetry [10]. Due to its unique spin-momentum-locked electronic structure, there are a number of unconventional anomalous magnetic response predicted in altermagnets, such as the anomalous Hall effect [8,14] and Kerr effect [15,16], which have been verified by experiments [17]. Moreover, very recently, the spin-splitting electronic structure was reported experimentally in MnTe through angle-resolved photoemission spectroscopy measures, which provides direct evidence for altermagnetism [18]. In terms of application, due to the advantages of the absence of stray field, terahertz spin dynamics, and strong $T$-symmetry breaking, altermagnets hold great promise for applications in spintronics. It has been suggested that the giant/tunneling magnetoresistance effect [19] and spin-splitter torque [20] can be generated in altermagnets.

So far, a wide range of materials have been classified as altermagnets, such as $RuO_2$ [8], MnTe [18,21], $MnF_2$ [9], and so on. However, the majority of reported altermagnets are three-dimensional (3D), while there are few reports on two-dimensional (2D) altermagnets. It has been shown that monolayer $MnP(S,Se)_3$ can transform from antiferromagnetism to altermagnetism by applying an electric field or through a Janus structure, which breaks the inversion symmetry between one sublattice and another [22]. Furthermore, some 2D altermagnets have been theoretically predicted, such as $V_2Te_2O$ [23] and $RuF_4$ [24]. It has been proposed that magnon-mediated superconductivity may occur in 2D altermagnets and the critical temperature can be enhanced by tuning the chemical potential [25]. However, to date, no specific material exhibiting altermagnetism has been demonstrated to show this result experimentally. Therefore, the search for 2D materials with altermagnetism is crucial for a deeper understanding of the fundamental physical properties inherent in 2D altermagnets.

On the other hand, 3D altermagnetism has been described by the spin Laue group in previous research [10], whereas how to describe 2D altermagnetism has not been solved. On the basis of Laue group and spin-group formalism, which considers symmetry transformation in decoupled real and spin space, it has been suggested that there are 32 nontrivial spin Laue groups, which correspond to three distinct magnetic phases. According to the characteristics of spin-momentum locking, the 10 nontrivial spin Laue groups of altermagnetism are classified into two types, the plane and bulk. Five plane spin Laue groups are considered to appear in both two-dimensional and three-dimensional crystals, whereas the five bulk spin Laue groups are thought to appear only in three-dimensional crystals. Here, we discover that there are seven spin groups to describe the spin-momentum locking in 2D altermagnets, rather than five spin Laue groups. The unexpected spin groups were previously classified as the bulk type.

In fact, the significance of altermagnetism in 2D materials remains an open question. As stated by the Mermin-Wagner theorem [26], magnetic anisotropy originating from spin-orbit coupling (SOC) is essential for magnetic order in 2D materials at finite temperatures. The impact of SOC on $RuF_4$, identified as a 2D altermagnet, has been discussed. It has been

*Contact author: zhaoyj@scut.edu.cn

 

proposed that in the presence of SOC, 2D altermagnets may exhibit weak ferromagnetism and SOC-induced band splitting [27]. Nevertheless, in our theoretical analysis and density functional theory (DFT) calculations, we have neglected the SOC effect, given the nonrelativistic origin of altermagnetism. However, to be more rigorous, we also provide a comparison of band structures with and without SOC in Appendix B.

In this work, we focus on the description and classification of 2D altermagnetism. Utilizing a method similar to that used to deduce the spin group theory, we have explored the two-dimensional spin layer group, which is grounded in the layer group concept. The spin layer groups are clearly beneficial for the search for 2D altermagnets and further understanding of 2D altermagnetism. We opt for layer groups, rather than point groups, as the symmetry transformations in real space for two main reasons. First, the 2D materials we commonly study are not strictly two-dimensional, but quasi-two-dimensional. Second, employing point groups can introduce ambiguity. Consequently, we believe that layer groups provide a more accurate symmetry description for 2D materials. To verify our results, we employ spin layer groups that describe altermagnetism to search for potential materials with 2D altermagnetism in the Materials Project database [28] and to classify the reported 2D altermagnets.

This paper is organized as follows: in Sec. II, we illustrate the process of deducing spin layer groups. In Sec. III, we provide some examples of 2D altermagnets to verify our result and analyze their spin-momentum-locking properties. Finally, we present our conclusions and offer some prospects about 2D altermagnetism.

## II. DERIVATION OF SPIN LAYER GROUPS

As is well known, a spin group is expressed as the direct product $r_s \otimes R_s$, where $r_s$ represents a spin-only group containing symmetry transformations acting on spin space and $R_s$ represents a nontrivial spin group containing pairs of transformations $[R_i||R_j]$, in which the transformations to the left of the double bar act on only the spin space and those to the right of the double bar act on only the real space. For collinear spin arrangements, the spin-only group mainly includes two transformations [10]. One is all rotations in spin space around the common axis of spins $C_\infty$, which make spin a good quantum number, so the band structure can be strictly separated into spin-up and spin-down channels. The other is a twofold rotation around an axis perpendicular to the spins, combined with the inversion symmetry of spin space $\overline{C_2}$, which is always accompanied by time-inversion symmetry $T$ and can be written as $[\overline{C_2}||T]$. When we apply it to the spin- and momentum-dependent bands, $[\overline{C_2}||T]\varepsilon(s,\mathbf{k}) = \varepsilon(s,-\mathbf{k})$ can be obtained. We provide a schematic diagram in Fig. 1 for a better understanding of the effect of various spin symmetries on the $\varepsilon(s,\mathbf{k})$ spectrum. Therefore, this transformation is equivalent to the real-space inversion in reciprocal space. Meanwhile, because this transformation makes the whole system invariant, for all collinear magnets, we can obtain $[\overline{C_2}||T]\varepsilon(s,\mathbf{k}) = \varepsilon(s,\mathbf{k})$, and thus, $\varepsilon(s,\mathbf{k}) = \varepsilon(s,-\mathbf{k})$. It can thus be concluded that under real-space inversion, the nonrelativistic band structure remains invariant for all collinear magnets, regardless of whether the system possesses real-space inversion symmetry. This conclusion is significant, as can be seen later, greatly simplifying the derivation of the spin layer group.

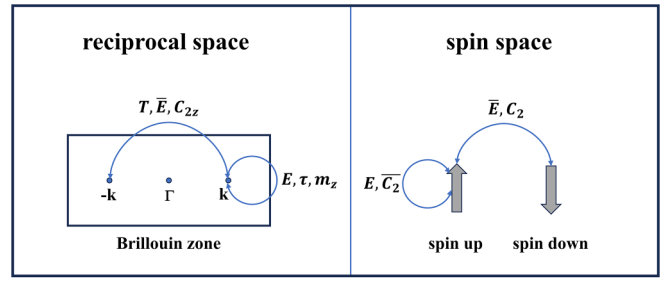


FIG. 1. Schematic diagram of the effect of various spin symmetries on the $\varepsilon(s,\mathbf{k})$ spectrum. In reciprocal space, $T$, $\overline{E}$, and $C_{2z}$ represent time-inversion symmetry, space-inversion symmetry, and twofold rotational symmetry around the $z$ axis, respectively. They will map the $k$ vector to its opposite number. $E$, $\tau$, and $m_z$ represent identity, translation symmetry, and mirror symmetry parallel to the $xy$ plane, and they will map the $k$ vector to itself. In spin space, $\overline{E}$ and $C_2$ represent inversion symmetry and twofold rotational symmetry on an axis perpendicular to the spins, respectively. They will transform the spin to the opposite one, while the identity symmetry $E$ and a twofold rotation around an axis perpendicular to the spins, combined with inversion symmetry of spin space $\overline{C_2}$, will make it invariant.

We now focus on the nontrivial spin group. The nontrivial spin group involves pairs of transformations $[R_i||R_j]$, which act independently on spin space and real space. Regarding the spin-space symmetry, for collinear spin arrangements, we select two transformations. One is the identity $E$ of the spin space, and the other is a twofold rotation around an axis perpendicular to the spins, denoted as $C_2$. Alternatively, spin-space inversion can also be chosen. These options result in the formation of two spin-space groups, $S_1 = \{E\}$ and $S_2 = \{E, C_2\}$.

Next, we address the real-space transformations within the nontrivial spin group. First of all, we assume that the 2D material under consideration lies parallel to the $xy$ plane. For the reasons mentioned earlier, we select the layer group to be the real-space group to construct the nontrivial spin layer group. Detailed information on layer groups can be found in [29]. As the prominent property of altermagnetism we focus on is spin-momentum locking, which is independent of real-space translation symmetry, we consider only the point group symmetry operator of layer group symmetry. For example, the glide reflection through the $xy$ plane is regarded as mirror symmetry through the $xy$ plane regardless of the translation direction. Similarly, the screw rotation around the $x$ axis is regarded as a twofold rotation around the $x$ axis. As stated above, for all collinear magnets with or without real-space inversion symmetry, the nonrelativistic band structure will be invariant when applied with real-space inversion symmetry operations. To avoid confusion between layer group symmetry and the symmetry that keeps band structure invariant, we refer to the latter as reciprocal-space symmetry. Through the direct product of the space-inversion group and the layer groups, we can obtain all reciprocal-space groups that correspond to the 80 layer groups, as listed in Table I. In fact, these groups belong to the Laue groups.

TABLE I. All reciprocal-space symmetries corresponding to layer groups. The plus (+) and minus (−) signs denote the counterclockwise and clockwise rotations, respectively. A bar above a symbol denotes inversion symmetry. For example, $\overline{C_{4z}^{+}}$ denotes 90° rotation counterclockwise with space inversion. A sequence of three numbers denotes the direction of the axis or plane. The direct product is denoted by ⊗.

| Reciprocal-space group | Layer groups | Reciprocal-space symmetry |
|---|---|---|
| 1 | 1–2 | $E, \overline{E}$ |
| 2 | 3–7 | $E, \overline{E}, C_{2z}, m_z$ |
| 3 | 8–18 | $E, \overline{E}, C_{2x}, m_x$ |
| 4 | 19–48 | $E, \overline{E}, C_{2z}, m_z, C_{2x}, m_x, C_{2y}, m_y$ |
| 5 | 49–52 | $E, \overline{E}, C_{2z}, m_z, C_{4z}^{+}, C_{4z}^{-}, \overline{C_{4z}^{+}}, \overline{C_{4z}^{-}}$ |
| 6 | 53–64 | $E, \overline{E}, C_{2z}, m_z, C_{4z}^{+}, C_{4z}^{-}, \overline{C_{4z}^{+}}, \overline{C_{4z}^{-}}, C_{2x}, m_x, C_{2y}, m_y, C_2^{110}, m_{110}, C_2^{1\bar{1}0}, m_{1\bar{1}0}$ |
| 7 | 65–66 | $E, \overline{E}, C_{3z}^{+}, C_{3z}^{-}, \overline{C_{3z}^{+}}, \overline{C_{3z}^{-}}$ |
| 8 | 67–72 | $E, \overline{E}, C_{3z}^{+}, C_{3z}^{-}, \overline{C_{3z}^{+}}, \overline{C_{3z}^{-}}, C_2^{110}, m_{110}, C_{2x}, C_{2y}, m_{\bar{2}10}, m_{\bar{1}20}$ |
| | | $(E, \overline{E}, C_{3z}^{+}, C_{3z}^{-}, \overline{C_{3z}^{+}}, \overline{C_{3z}^{-}}, C_2^{1\bar{1}0}, C_2^{120}, C_2^{210}, m_{1\bar{1}0}, m_x, m_y)$ |
| 9 | 73–75 | $E, \overline{E}, C_{3z}^{+}, C_{3z}^{-}, \overline{C_{3z}^{+}}, \overline{C_{3z}^{-}}, C_{2z}, m_z, C_{6z}^{+}, \overline{C_{6z}^{+}}, C_{6z}^{-}, \overline{C_{6z}^{-}}$ |
| 10 | 76–80 | $\{E, \overline{E}\} \otimes \{E, C_{3z}^{+}, C_{3z}^{-}, C_{2z}, C_{6z}^{+}, C_{6z}^{-}, C_2^{110}, C_{2x}, C_{2y}, C_2^{1\bar{1}0}, C_2^{120}, C_2^{210}\}$ |

According to the isomorphism theorem [12], which implies decomposition with the same number of cosets for the two groups, the nontrivial spin layer group can be classified as three types, corresponding to three magnetic phase. Selecting $S_1$ as the transformation for the spin space, a unique scenario exists in which the nontrivial spin layer group $R_1 = [S_1||G]$ can be derived, with $G$ representing the layer groups. This nontrivial spin layer group describes nonzero magnetization and band structure with broken time-inversion symmetry, corresponding to ferromagnetism.

Similarly, if we choose $S_2$ to be the spin-space transformation, two cases will appear. In one the nontrivial spin layer group is given by $R_2 = [S_2||G] = [E||G] + [C_2||G]$, which describes zero magnetization and a spin-degenerate band structure with time-inversion symmetry, corresponding to antiferromagnetism. In the other the nontrivial spin layer group is given by $R_3 = [E||H] + [C_2||G - H]$, where $H$ is a halving subgroup of layer group $G$. This describes zero magnetization and a band structure with broken time-inversion symmetry, corresponding to altermagnetism, which we will focus on later. The transformation associated with the spin-space identity will link atoms within the same sublattice, whereas the transformation involving a twofold rotation in spin space will connect atoms in one sublattice to those of the opposite sublattice.

In 2D systems, certain symmetries protect the spin degeneracy of the nonrelativistic band structure for all $\mathbf{k}$ vectors in the whole Brillouin zone. First, $[C_2||\tau]$ symmetry obviously implies spin degeneracy of the band structure, where $\tau$ is translation symmetry connecting atoms of the opposite sublattices. As the spin degeneracy is independent of real-space translation symmetry, $[C_2||\tau]$ is equivalent to $[C_2||E]$, which means $[C_2||E]\varepsilon(s, \mathbf{k}) = \varepsilon(-s, \mathbf{k}) = \varepsilon(s, \mathbf{k})$. Moreover, the spin degeneracy is also protected by the inversion symmetry connecting atoms of the opposite sublattices, i.e., $[C_2||\overline{E}]$. This is because $[\overline{C_2}||T]$ is a spin-only symmetry and the spin (layer) group is a direct product of the spin-only group and nontrivial spin (layer) group, i.e., $[C_2||\overline{E}][\overline{C_2}||T] = [\overline{E}||T\overline{E}]$, which is $\mathcal{PT}$ symmetric to protect Kramers spin degeneracy. These results were reported previously [10]. For 2D symmetry, however, there are two extra symmetries to protect Kramers spin degeneracy. The first one is $[C_2||m_z]$, which represents the case in which the atoms of opposite sublattices can be connected by the mirror symmetry through the $xy$ plane. In this case, we can obtain $[C_2||m_z]\varepsilon(s, \mathbf{k}) = \varepsilon(-s, \mathbf{k})$. Meanwhile, $[C_2||m_z]$ is also the symmetry of the system, i.e., $[C_2||m_z]\varepsilon(s, \mathbf{k}) = \varepsilon(s, \mathbf{k})$. Therefore, spin degeneracy of the band structure will appear in materials with $[C_2||m_z]$ symmetry. The second one is $[C_2||C_{2z}]$, which represents the case in which the atoms of the opposite sublattices can be connected by a twofold rotation around the $z$ axis. It can be found that the product of $[C_2||C_{2z}]$ and the spin-only symmetry $[\overline{C_2}||T]$ equals $[\overline{E}||TC_{2z}]$. This means that $[\overline{E}||TC_{2z}]\varepsilon(s, \mathbf{k}) = \varepsilon(-s, \mathbf{k}) = \varepsilon(s, \mathbf{k})$, so spin-degenerate band structure is protected in 2D materials with $[\overline{E}||TC_{2z}]$ symmetry. These symmetries were also suggested to protect spin degeneracy in a recent work [24]. These four symmetries must be excluded when we deduce the nontrivial spin layer group for altermagnetism. If a 2D material possesses any of the crystal symmetries $\{\tau, m_z, \overline{E}, C_{2z}\}$ in real space, this symmetry must be accompanied by a spin-space identity in the altermagnetic phase. Therefore, the atoms of the opposite sublattices cannot be connected by any of the crystal symmetries $\{\tau, m_z, \overline{E}, C_{2z}\}$ in 2D altermagnets.

Next, we focus on constructing the nontrivial spin layer groups to describe altermagnetism, starting with the formalism $R_3 = [E||H] + [C_2||G - H]$ and the reciprocal-space groups coming from the layer groups. We finally obtain seven nontrivial spin layer groups, as listed in Table II. Here, we adopt Litvin's notation for the spin groups [13], in which a superscript 1 represents the identity symmetry in spin space and a superscript 2 represents the rotation symmetry $C_2$ in spin space. Notably, some reciprocal-space groups are incapable of forming a nontrivial spin layer group for altermagnetism because they lack the appropriate halving subgroup. This deficiency necessitates that the symmetries, $E, m_z, \overline{E}$, and $C_{2z}$, should be accompanied by a spin-space identity to prevent spin degeneracy if these symmetries are present in the

TABLE II. All nontrivial spin layer groups, corresponding layer groups, corresponding reciprocal-space groups (RGs), the basic characteristic of spin-momentum locking, and material candidates. Here, we adopt Litvin's notation of the spin groups. The asterisk (*) denotes that the material is predicted by symmetry analysis in this work and the evidence of altermagnetism can be found in Sec. III. The other materials have been reported in the previous research.

| Nontrivial spin layer group | Spin-momentum locking ($k_x$, $k_y$) | Layer group | RG | Material candidate |
|---|---|---|---|---|
| ${}^{2}2/{}^{2}m_x$ | 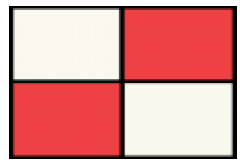 | 8–18 | 3 | $RuF_4$ [24,27] |
| ${}^{2}m{}^{2}m{}^{1}m$ | | 19–48 | 4 | $MnTeMoO_6^*$ |
| ${}^{2}4/{}^{1}m$ | 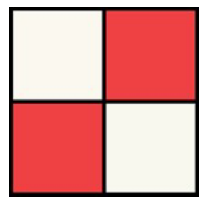 | 49–52 | 5 | |
| ${}^{2}4/{}^{1}m{}^{2}m{}^{1}m$ | | 53–64 | 6 | $V_2Se_2O$ [5], $V_2Te_2O$ [23], $Cr_2O_2$ [30,31] |
| ${}^{1}4/{}^{1}m{}^{2}m{}^{2}m$ | 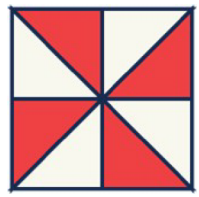 | 53–64 | 6 | $VP_2H_8(NO_4)_2^*$ |
| ${}^{1}\bar{3}{}^{2}m$ | 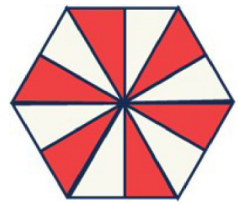 | 67–72 | 8 | $Mn_2P_2S_3Se_3$ [22] |
| ${}^{1}6/{}^{1}m{}^{2}m{}^{2}m$ | | 76-80 | 10 | |

real-space group. Therefore, not all layer groups can be constructed to nontrivial spin layer groups, as listed in Table II. For example, the second reciprocal-space group in Table I possesses four symmetries, $\{E, m_z, \overline{E}, C_{2z}\}$, all of which must be accompanied by a spin-space identity when constructing a nontrivial spin layer group for altermagnetism. Therefore, this reciprocal-space group cannot be constructed to nontrivial spin layer group. It is worth noting that the five spin Laue groups describing 2D materials in previous research are all included within the seven spin layer groups. Interestingly, two results not previously categorized as plane-type altermagnetism have emerged. One case is the nontrivial spin layer group ${}^{2}2/{}^{2}m_x$, i.e., $R_3 = [E||\{E, \overline{E}\}] + [C_2||\{C_{2x}, m_x\}]$, which exhibits the same spin-momentum-locking characteristics as the group ${}^{2}m{}^{2}m{}^{1}m$, previously identified as plane-type altermagnetism. We also find that it can be understood as the spin Laue group ${}^{2}2/{}^{2}m$ in the case where the twofold rotation symmetry is around the $x$ axis. This is because the $[C_2||m_z]$ symmetry, which preserves the spin-degenerate band in the whole Brillouin zone, disappears in this case. By symmetry analysis, we find that the material $RuF_4$ exhibits the symmetries in this group, as described in Sec. III. The other is group ${}^{1}\bar{3}{}^{2}m$, i.e., $R_3 = [E||\{E, \overline{E}, C_{3z}^{+}, C_{3z}^{-}, \overline{C_{3z}^{+}}, \overline{C_{3z}^{-}}\}] + [C_2||\{C_2^{110}, m_{110}, C_{2x}, C_{2y}, m_{\bar{1}10}, m_{\bar{1}20}\}]$, which has been classified as bulk-type altermagnetism in three-dimensional altermagnetism. However, it is the absence of the $[C_2||m_z]$ and $[C_2||C_{2z}]$ symmetries that make it appear in the seven spin layer groups. In two-dimensional altermagnetism, it has the same spin-momentum-locking properties as the group ${}^{1}6/{}^{1}m{}^{2}m{}^{2}m$, given that the $\overline{C_{3z}^{+}}$ symmetry is equivalent to $C_{6z}^{-}$ in two-dimensional reciprocal space. Additionally, we have identified that $Mn_2P_2S_3Se_3$, with a Janus structure, exhibits the symmetries in this group, a topic that will be discussed further in the following section. In summary, we have derived spin layer groups by combining the spin group and layer groups to describe 2D altermagnetism and have provided their corresponding layer groups. In the next section, we will give some examples of 2D altermagnets and discuss their spin-momentum-locking properties.

## III. SPIN-MOMENTUM LOCKING IN MATERIAL CANDIDATES

We now focus on the main characteristic of spin-momentum locking in 2D altermagnets, and subsequently, we will provide examples of the above-derived spin layer groups in altermagnetism and discuss their characteristic of spin-momentum locking. Symmetry enables us to obtain information about the band structure, such as the

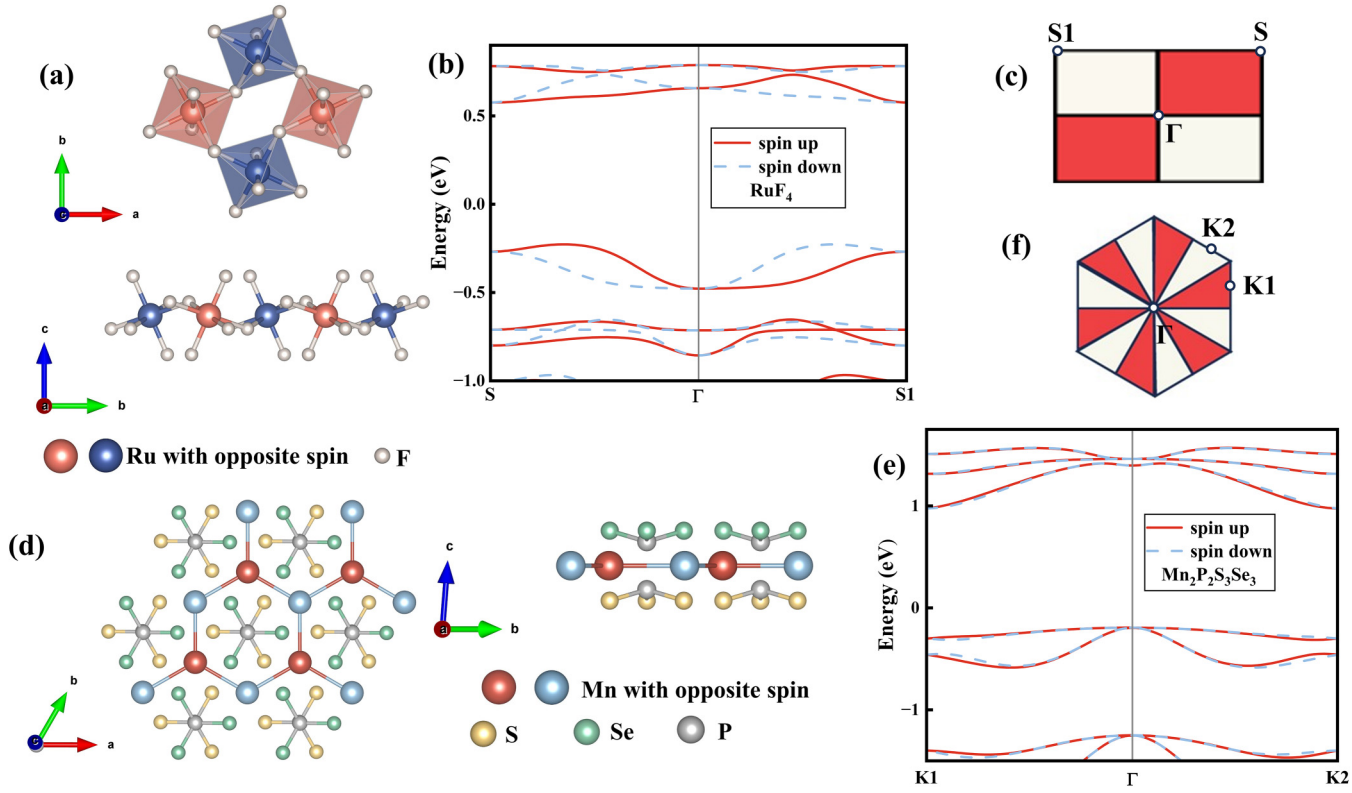


FIG. 2. The crystal structure and nonrelativistic band structure of $RuF_4$ and $Mn_2P_2S_3Se_3$. (a) and (d) The crystal structure of $RuF_4$ and $Mn_2P_2S_3Se_3$, where different colors of magnetic atoms represent the opposite spin sublattices. (b) and (e) The band structure of $RuF_4$ and $Mn_2P_2S_3Se_3$ without SOC, where the red solid line and blue dashed line represent the opposite spin channels. (c) and (f) The **k** path we use to calculate the band structure. The different colors represent opposite spins.

spin-degenerate **k** vector and nodal line, prior to calculating the band structure. First of all, the spin-degenerate nodal line is protected by the $[C_2||G-H]$ symmetry in $R_3$, particularly when this symmetry transforms the wave vector on this line into itself, i.e., $[C_2||G-H]\varepsilon(s,\mathbf{k})=\varepsilon(-s,\mathbf{k})=\varepsilon(s,\mathbf{k})$. For instance, the $[C_2||C_{2x}]$ symmetry, where $C_{2x}$ is a twofold rotation around the $x$ axis, determines a spin-degenerate nodal line along the $x$ axis. Moreover, if a symmetry $[C_2||G-H]$ in $R_3$ transforms a wave vector into itself or another wave vector separated by a reciprocal lattice vector, the band structure at this **k** vector will exhibit spin degeneracy. A typical example is the band structure at the Γ point, which is consistently spin degenerate because any symmetry of $[C_2||G-H]$ transforms the Γ point into itself. Meanwhile, opposite spins will appear at two distinct **k** vectors which can be connected by the symmetry of $G-H$. This occurs because $[C_2||G-H]\varepsilon(s,\mathbf{k})=\varepsilon(-s,\mathbf{k}')$, where **k** can be changed to $\mathbf{k}'$ by the symmetry in $G-H$. This outcome is instrumental for determining the opposite spin-splitting **k** vectors during the calculation of the band structure. The fundamental characteristic of spin-momentum locking for each spin layer group is listed in the second column of Table II.

On the basis of the spin layer group, we classify the reported 2D altermagnets as listed in Table II. It is observed that these materials mostly correspond to the spin layer group ${}^{2}4/{}^{1}m^{2}m^{1}m$. Furthermore, there are materials that exemplify two unexpected spin layer groups, which serve to validate our aforementioned results. $RuF_4$ is composed of Ru atoms located at the center of an octahedron formed by F atoms, as shown in Fig. 2(a). Its layer group is No. 18, which contains the identity operation $E$, a twofold rotation symmetry around the $x$ axis $C_{2x}$, mirror symmetry through the $yz$ plane $m_x$, and real-space inversion symmetry $\overline{E}$. We also provide the magnetic configuration in the altermagnetic state in Fig. 2(a). Through symmetry analysis, it is demonstrated that atoms with opposite magnetic moment can be connected by $C_{2x}\tau$ and $m_x\tau$, where $\tau$ is a translation by half the lattice vector. Additionally, atoms with the same magnetic moment are connected by space-inversion symmetry. Consequently, its spin layer group is identified as ${}^{2}2/{}^{2}m_x$, and the **k** path $\Gamma-S$ exhibits a spin sign opposite that of $\Gamma-S1$. The employed **k** path is displayed in Fig. 2(c). Figure 2(b) provides the nonrelativistic band structure of $RuF_4$, which corroborates the analysis results mentioned above.

The monolayer $Mn_2P_2S_3Se_3$ with a Janus structure was identified as a 2D altermagnet in a previous report [22]. Within the framework of the spin layer group, it can be classified as ${}^{1}\overline{3}{}^{2}m$. In Fig. 2(d), we illustrate the crystal structure of $Mn_2P_2S_3Se_3$, where all S atoms are below the Mn plane and all Se atoms are above it and the magnetic configuration is in an altermagnetic state. Through symmetry analysis, it is revealed that $Mn_2P_2S_3Se_3$ belongs to layer group 70, which contains threefold rotation symmetry around the $z$ axis and three mirror symmetries through the planes perpendicular to the $xy$ plane, and atoms with opposite magnetic moments can be connected by mirror symmetry through a plane

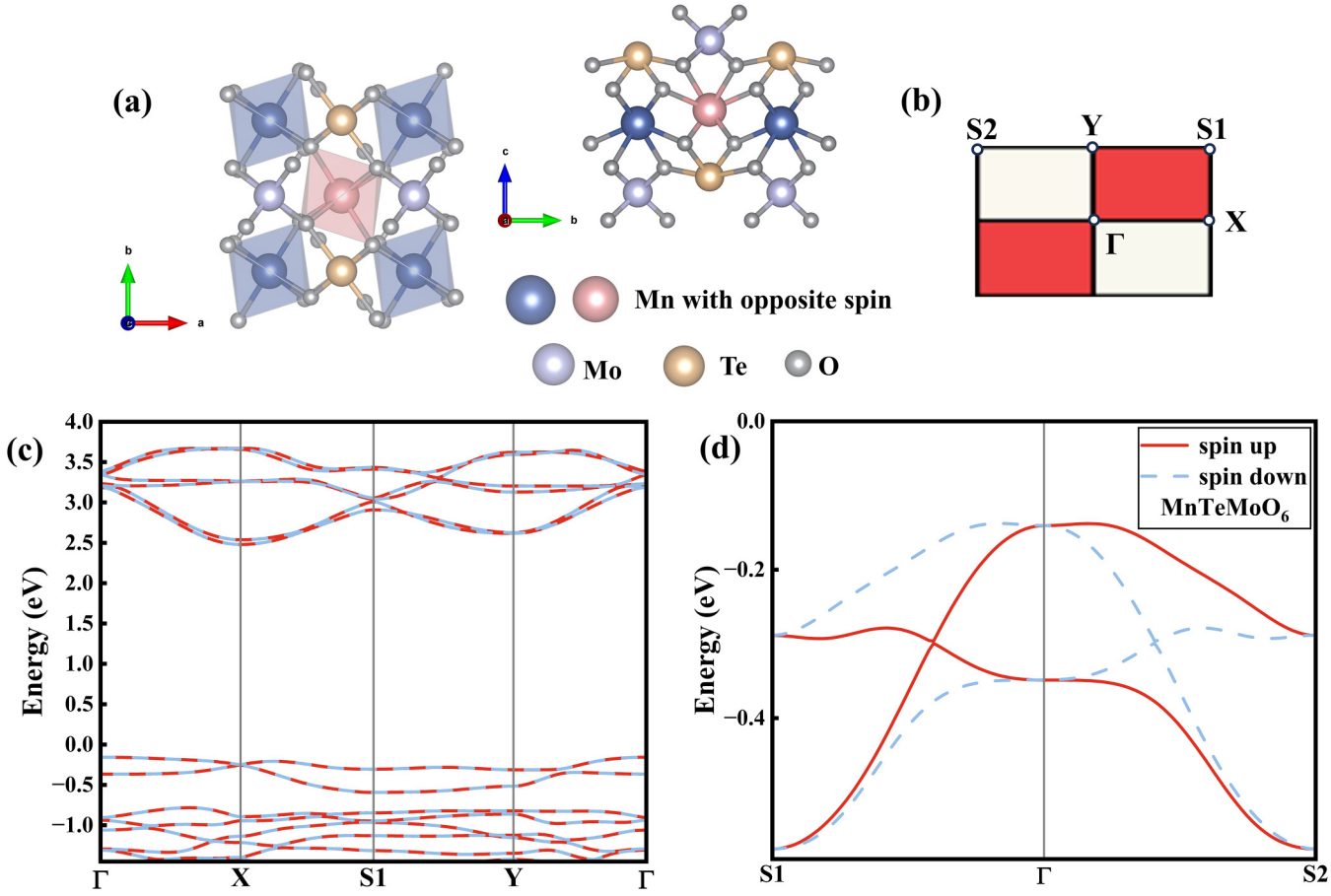


FIG. 3. The crystal structure and nonrelativistic band structure of $MnTeMoO_6$. (a) The crystal structure of $MnTeMoO_6$, where pink and blue represent the opposite spin sublattices. (b) The Brillouin zone of $MnTeMoO_6$, in which the different colors represent opposite spins, and high-symmetry points used to calculate band structure. (c) The band structure of $MnTeMoO_6$ without SOC along the **k** path $\Gamma$-$X$-$S1$-$Y$-$\Gamma$ is spin degeneracy, where red solid lines and blue dashed lines represent the opposite spin channels. (d) The band structure of $MnTeMoO_6$ without SOC along the **k** path $S1$-$\Gamma$-$S2$ is spin splitting, where red solid lines and blue dashed lines represent the opposite spin channels. (c) and (d) clearly exhibit the basic characteristic of spin-momentum locking of spin layer group ${}^2m^2m^1m$.

perpendicular to the $xy$ plane. Therefore, its spin layer group is ${}^1\bar{3}^2m$, and the **k** path $\Gamma - K1$ exhibits a spin sign opposite that of $\Gamma - K2$. The **k** path utilized in our analysis is shown in Fig. 2(f). Figure 2(e) provides the band structure of $Mn_2P_2S_3Se_3$, which confirms the basic characteristic of spin-momentum locking with spin layer group ${}^1\bar{3}^2m$.

However, four spin layer groups lack corresponding materials. We employ the symmetry operation in the spin layer group to search for the material candidates of these four groups in the Materials Project database. For a specific spin layer group, we first selected materials containing transition metal elements belonging to space groups that correspond to this spin layer group [32,33] within the Materials Project database. Then, we screened these materials individually. If a material with a van der Waals structure had an antiferromagnetic configuration, we performed a symmetry analysis to determine whether it is an altermagnet or not. Once we identified a material candidate for a spin layer group, we ceased our search for that group and initiated the search for the next spin layer group using the aforementioned process. That was because our aim was to identify a material candidate for each spin layer group, rather than searching for all 2D altermagnets in the Materials Project database. All of these operations were performed manually, without using any algorithms. It is suggested that monolayer $MnTeMoO_6$ has the spin layer group ${}^2m^2m^1m$ and $VP_2H_8(NO_4)_2$ has ${}^14/{}^1m^2m^2m$; these were not reported in previous studies. Nevertheless, we have not identified potential materials for the spin layer groups ${}^24/{}^1m$ and ${}^16/{}^1m^2m^2m$, likely due to their high symmetry requirements. Of course, we believe that these two spin layer groups exist, as they are also represented within the spin Laue group.

The crystal structure of $MnTeMoO_6$ is schematically illustrated in Fig. 3(a), where pink and blue represent real-space sublattices with opposite spins in altermagnetism. As a van der Waals material, it can be exfoliated from the bulk compound. Our DFT calculations reveal that the energy of the altermagnetic state is 8.5 meV per magnetic atom lower than that of the ferromagnetic state. Therefore, its magnetic ground state is the altermagnetic state. Its layer group is No. 21, which contains twofold rotation symmetry around the $z$ axis and two screw rotations around the $x$ and $y$ axes, and its spin layer group is ${}^2m^2m^1m$. The sublattices can be related by a twofold

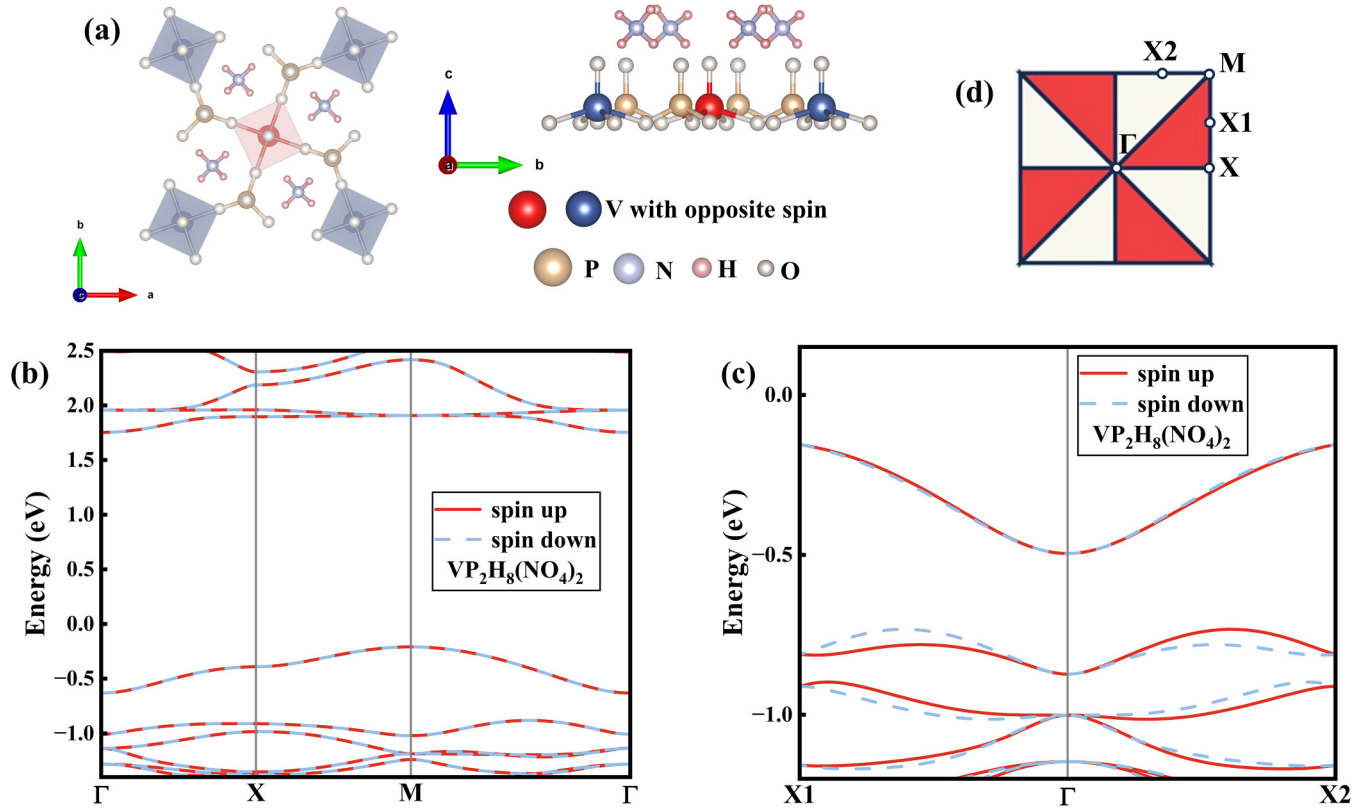


FIG. 4. The crystal structure and nonrelativistic band structure of $VP_2H_8(NO_4)_2$. (a) The crystal structure of $VP_2H_8(NO_4)_2$, where red and blue represent the opposite spin sublattices. (b) The band structure of $VP_2H_8(NO_4)_2$ without SOC along the **k** path $\Gamma$-$X$-$M$-$\Gamma$ is spin degeneracy, where red solid lines and blue dashed lines represent the opposite spin channels. (c) The band structure of $VP_2H_8(NO_4)_2$ without SOC along the **k** path $X1$-$\Gamma$-$X2$ is spin splitting, where red solid lines and blue dashed lines represent the opposite spin channels. (b) and (c) clearly exhibit the basic characteristic of spin-momentum locking of spin layer group ${}^{1}4/{}^{1}m^{2}m^{2}m$. (d) The Brillouin zone of $VP_2H_8(NO_4)_2$, in which the different colors represent opposite spins, and high-symmetry points used to calculate band structure.

rotation around the $x$ axis (or $y$ axis) with translation, and the twofold rotation around the $z$ axis maps the sublattice to itself. Therefore, the spin-momentum locking of $MnTeMoO_6$ is determined by the symmetry of $[C_2||C_{2x}]$ ($[C_2||C_{2y}]$); i.e., the spin-degenerate nodal line at $k_x = 0$ ($k_y = 0$) is protected by $[C_2||C_{2x}]$ ($[C_2||C_{2y}]$). The **k** paths, related by $C_{2x}$ ($C_{2y}$) but not separated by a reciprocal lattice vector, have opposite spin signs. Figures 3(c) and 3(d) show the DFT-calculated nonrelativistic band structure, and the employed **k** paths are shown in Fig. 3(b). When we selected a high-symmetry path along $\Gamma$-$X$-$S1$-$Y$-$\Gamma$ to calculate the band structure, we obtained only spin-degenerate bands, as illustrated in Fig. 3(c); they are protected by $[C_2||C_{2x}]$ ($[C_2||C_{2y}]$) symmetry. However, it is observed that the band structure of **k** path $S1 - \Gamma - S2$ is spin splitting with the $\Gamma - S1$ path having a spin opposite that of $\Gamma - S2$. This is a typical altermagnetic characteristic. These results are consistent with the conclusions we reached earlier in our discussion.

For spin layer group ${}^{1}4/{}^{1}m^{2}m^{2}m$, we identified $VP_2H_8(NO_4)_2$ as exhibiting this symmetry. Its layer group is No. 56, which contains a fourfold rotation symmetry around the $z$ axis, a mirror symmetry through the (110) plane, and three glide reflections through the $xz$ plane, $yz$ plane, and $(1\bar{1}0)$ plane. The crystal structure of $VP_2H_8(NO_4)_2$ is schematically illustrated in Fig. 4(a), with red and blue representing real-space sublattices with opposite spins in altermagnetism. Being a van der Waals material, it can be exfoliated from the bulk compound. We found that the energy of the altermagnetic state is 0.47 meV per magnetic atom lower than that of the ferromagnetic state using DFT calculations, indicating that its magnetic ground state is an altermagnetic state. The sublattices can be related by reflection through the $xz$ plane [$yz$ plane, (110) plane, or $(1\bar{1}0)$ plane], and a fourfold rotation around the $z$ axis maps the sublattice to itself. Consequently, the spin-momentum locking of $VP_2H_8(NO_4)_2$ is determined by the $[C_2||\{m_x, m_y, m_{110}, m_{1\bar{1}0}\}]$ symmetries. That is, the spin-degenerate nodal lines at $k_x = 0$ and $k_y = 0$ are protected by $[C_2||m_x]$ and $[C_2||m_y]$. The **k** paths, related by $m_x$ ($m_y, m_{110}, m_{1\bar{1}0}$) but not separated by a reciprocal lattice vector, have opposite spin signs. Figures 4(b) and 4(c) show the DFT-calculated band structure without SOC, and the employed **k** paths are shown in Fig. 4(d). If we choose the high-symmetry path along $\Gamma$-$X$-$M$-$\Gamma$ to calculate the band structure, only the spin-degenerate bands are obtained, as illustrated in Fig. 4(b), which is protected by the $m_x$ and $m_{1\bar{1}0}$ symmetries. However, the band structure of the **k** path along $X1 - \Gamma - X2$ is spin splitting, and $\Gamma - X1$ has a spin opposite to that of $\Gamma - X2$, which is a typical altermagnetic characteristic. Again, these results are consistent with the conclusions we reached above.

TABLE III. The employed $U$ value and lattice constant. A dash (—) denotes that we did not apply the Hubbard $U$ correction to this material.

| Material | $U$ (eV) | $a$ (Å) | $b$ (Å) |
|---|---|---|---|
| $RuF_4$ | — | 5.42 | 5.09 |
| $Mn_2P_2S_3Se_3$ | — | 6.22 | 6.22 |
| $MnTeMoO_6$ | 3.9 (Mn), 4.38 (Mo) | 5.14 | 5.41 |
| $VP_2H_8(NO_4)_2$ | 3.25 (V) | 8.46 | 8.46 |

## IV. CONCLUSION

In summary, we constructed seven spin layer groups to describe and classify 2D altermagnetism, extending beyond the previously reported plane-type spin Laue group. We believe that spin layer groups will be helpful in the future search for 2D altermagnets. Meanwhile, we utilized these spin layer groups to identify material candidates, validating the use of symmetry in the search for 2D altermagnets. We also determined their magnetic ground state is the altermagnetic state and calculated the band structure by DFT calculations without SOC. Furthermore, we conducted a symmetry-based analysis to evaluate the spin-momentum-locking characteristics of the materials.

Nevertheless, several key issues require further investigation. First, the significance of altermagnetism in 2D materials remains an open question, necessitating further discussion and DFT calculations with SOC. Second, there has been a lack of experimental exploration of 2D altermagnets so far. Finally, determining whether the noncollinear magnetic state in altermagnetism differs from that in antiferromagnetism is a question that merits further exploration.

## ACKNOWLEDGMENTS

This work is financially supported by the National Natural Science Foundation of China (Grant No. 12074126). The computer times at the High Performance Computational Center at South China University of Technology are gratefully acknowledged. Y.-J.Z. is grateful for the valuable suggestions provided by Prof. J. Liu.

## APPENDIX A: COMPUTATIONAL DETAILS

All calculations were performed using the Vienna Ab initio Simulation Package (VASP) [34,35], employing the projector augmented wave method [36] based on density functional theory. For the exchange-correlation functional, we use the generalized gradient approximation with the Perdew-Burke-Ernzerhof functional [37], along with Hubbard $U$ correction [38]. The employed $U$ value and lattice constant are listed in Table III. A cutoff energy of 500 eV was set for the plane wave basis. The structure was relaxed until the forces on atoms were below 0.01 eV/Å and the convergence criterion was $1 \times 10^{-7}$ eV for the energy difference in the electronic self-consistent calculation. A vacuum of 15Å was constructed perpendicular to the material plane. The SOC effect was not considered in the calculations.

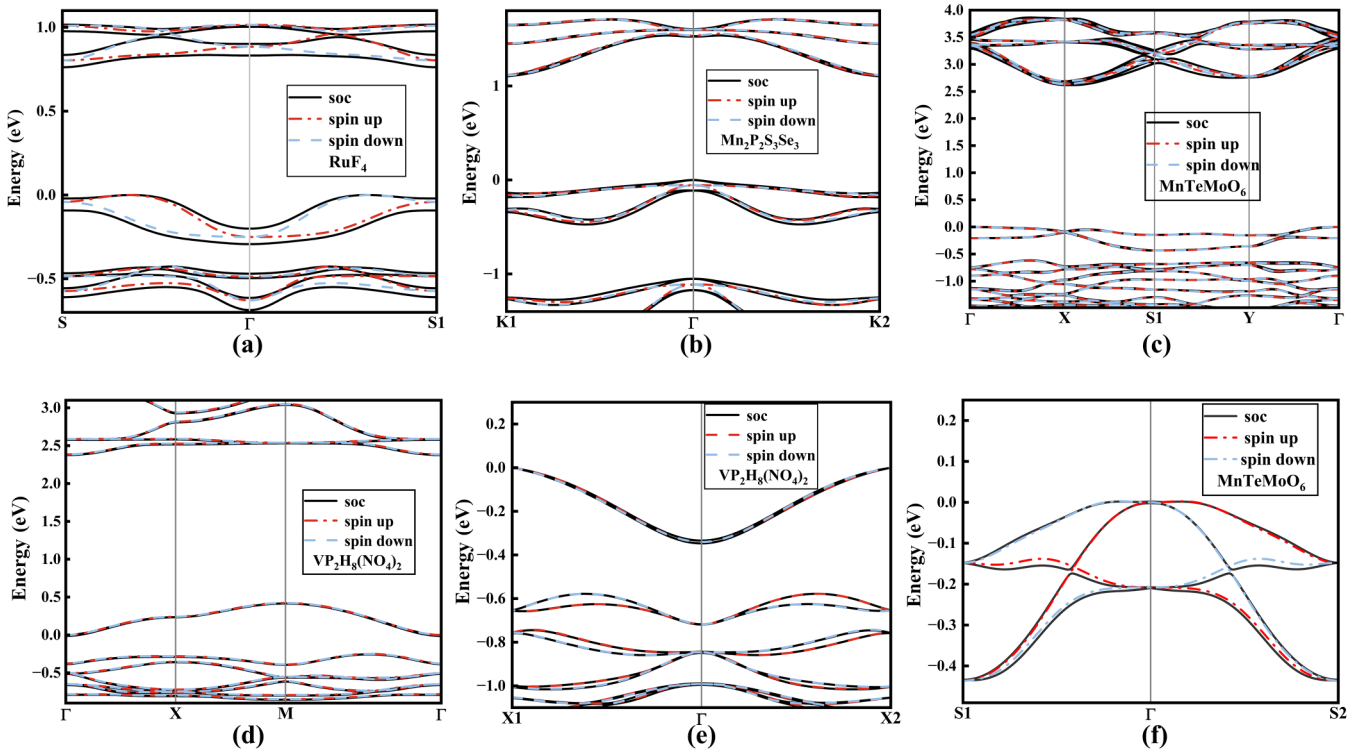


FIG. 5. The band structure with and without SOC of (a) $RuF_4$, (b) $Mn_2P_2S_3Se_3$, (c) and (f) $MnTeMoO_6$, and (d) and (e) $VP_2H_8(NO_4)_2$. The red and blue dashed lines represent the opposite channels, and the black solid lines represent band structure with SOC. (a) corresponds to Fig. 2(b). (b) corresponds to Fig. 2(e). (c) and (f) correspond to Figs. 3(c) and 3(d). (d) and (e) correspond to Figs. 4(b) and 4(c).

## APPENDIX B: COMPARISON OF BAND STRUCTURES WITH AND WITHOUT SOC

As is well known, the absence of the SOC effect is an approximation. In this Appendix, we provide a comparison of band structures with and without SOC for all materials, as illustrated in Fig. 5. It is implied that the magnitude of spin splitting originating from the SOC effect is smaller than that arising from altermagnetism. Therefore, altermagnetism plays a key role in spin splitting in these materials, and the discussion in the main text without SOC is appropriate. It is worth noting that the intersections of two bands in Fig. 3(d) vanish when we consider the SOC effect, as illustrated in Fig. 5(f). Consequently, we conclude that these points are not Weyl points.


[1] L. Šmejkal, J. Sinova, and T. Jungwirth, Emerging research landscape of altermagnetism, Phys. Rev. X **12**, 040501 (2022).

[2] X. Zhou, W. Feng, R.-W. Zhang, L. Šmejkal, J. Sinova, Y. Mokrousov, and Y. Yao, Crystal thermal transport in altermagnetic $RuO_2$, Phys. Rev. Lett. **132**, 056701 (2024).

[3] I. Mazin, Altermagnetism then and now, Physics **17**, 4 (2024).

[4] X. Chen, J. Ren, J. Li, Y. Liu, and Q. Liu, Spin space group theory and unconventional magnons in collinear magnets, arXiv:2307.12366.

[5] H.-Y. Ma, M. Hu, N. Li, J. Liu, W. Yao, J.-F. Jia, and J. Liu, Multifunctional antiferromagnetic materials with giant piezomagnetism and noncollinear spin current, Nat. Commun. **12**, 2846 (2021).

[6] I. I. Mazin, K. Koepernik, M. D. Johannes, R. González-Hernández, and L. Šmejkal, Prediction of unconventional magnetism in doped $FeSb_2$, Proc. Natl. Acad. Sci. USA **118**, e2108924118 (2021).

[7] S. Hayami, Y. Yanagi, and H. Kusunose, Momentum-dependent spin splitting by collinear antiferromagnetic ordering, J. Phys. Soc. Jpn. **88**, 123702 (2019).

[8] L. Šmejkal, R. González-Hernández, T. Jungwirth, and J. Sinova, Crystal time-reversal symmetry breaking and spontaneous Hall effect in collinear antiferromagnets, Sci. Adv. **6**, eaaz8809 (2020).

[9] L.-D. Yuan, Z. Wang, J.-W. Luo, E. I. Rashba, and A. Zunger, Giant momentum-dependent spin splitting in centrosymmetric low-$Z$ antiferromagnets, Phys. Rev. B **102**, 014422 (2020).

[10] L. Šmejkal, J. Sinova, and T. Jungwirth, Beyond conventional ferromagnetism and antiferromagnetism: A phase with nonrelativistic spin and crystal rotation symmetry, Phys. Rev. X **12**, 031042 (2022).

[11] W. Brinkman and R. J. Elliott, Theory of spin-space groups, Proc. R. Soc. London, Ser. A **294**, 343 (1966).

[12] D. B. Litvin and W. Opechowski, Spin groups, Physica (Amsterdam) **76**, 538 (1974).

[13] D. B. Litvin, Spin point groups, Acta. Crystallogr., Sect. A **33**, 279 (1977).

[14] L. Šmejkal, A. H. MacDonald, J. Sinova, S. Nakatsuji, and T. Jungwirth, Anomalous Hall antiferromagnets, Nat. Rev. Mater. **7**, 482 (2022).

[15] K. Samanta, M. Ležaić, M. Merte, F. Freimuth, S. Blügel, and Y. Mokrousov, Crystal Hall and crystal magneto-optical effect in thin films of $SrRuO_3$, J. Appl. Phys. **127**, 213904 (2020).

[16] X. Zhou, W. Feng, X. Yang, G.-Y. Guo, and Y. Yao, Crystal chirality magneto-optical effects in collinear antiferromagnets, Phys. Rev. B **104**, 024401 (2021).

[17] H. Bai, L. Han, X. Y. Feng, Y. J. Zhou, R. X. Su, Q. Wang, L. Y. Liao, W. X. Zhu, X. Z. Chen, F. Pan, X. L. Fan, and C. Song, Observation of spin splitting torque in a collinear antiferromagnet $RuO_2$, Phys. Rev. Lett. **128**, 197202 (2022).

[18] S. Lee, S. Lee, S. Jung, J. Jung, D. Kim, Y. Lee, B. Seok, J. Kim, B. G. Park, L. Šmejkal, C.-J. Kang, and C. Kim, Broken Kramers degeneracy in altermagnetic MnTe, Phys. Rev. Lett. **132**, 036702 (2024).

[19] L. Šmejkal, A. B. Hellenes, R. González-Hernández, J. Sinova, and T. Jungwirth, Giant and tunneling magnetoresistance in unconventional collinear antiferromagnets with nonrelativistic spin-momentum coupling, Phys. Rev. X **12**, 011028 (2022).

[20] R. González-Hernández, L. Šmejkal, K. Výborný, Y. Yahagi, J. Sinova, T. Jungwirth, and J. Železný, Efficient electrical spin splitter based on nonrelativistic collinear antiferromagnetism, Phys. Rev. Lett. **126**, 127701 (2021).

[21] R. D. Gonzalez Betancourt, J. Zubáč, R. Gonzalez-Hernandez, K. Geishendorf, Z. Šobáň, G. Springholz, K. Olejník, L. Šmejkal, J. Sinova, T. Jungwirth, S. T. B. Goennenwein, A. Thomas, H. Reichlová, J. Železný, and D. Kriegner, Spontaneous anomalous Hall effect arising from an unconventional compensated magnetic phase in a semiconductor, Phys. Rev. Lett. **130**, 036702 (2023).

[22] I. Mazin, R. González-Hernández, and L. Šmejkal, Induced monolayer altermagnetism in $MnP(S, Se)_3$ and FeSe, arXiv:2309.02355.

[23] Q. Cui, Y. Zhu, X. Yao, P. Cui, and H. Yang, Giant spin-Hall and tunneling magnetoresistance effects based on a two-dimensional nonrelativistic antiferromagnetic metal, Phys. Rev. B **108**, 024410 (2023).

[24] J. Sødequist and T. Olsen, Two-dimensional altermagnets from high throughput computational screening: Symmetry requirements, chiral magnons, and spin-orbit effects, Appl. Phys. Lett. **124**, 182409 (2024).

[25] B. Brekke, A. Brataas, and A. Sudbø, Two-dimensional altermagnets: Superconductivity in a minimal microscopic model, Phys. Rev. B **108**, 224421 (2023).

[26] N. D. Mermin and H. Wagner, Absence of ferromagnetism or antiferromagnetism in one- or two-dimensional isotropic Heisenberg models, Phys. Rev. Lett. **17**, 1133 (1966).

[27] M. Milivojević, M. Orozović, S. Picozzi, M. Gmitra, and S. Stavrić, Interplay of altermagnetism and weak ferromagnetism in two-dimensional $RuF_4$, 2D Mater. **11**, 035025 (2024).

[28] A. Jain, S. P. Ong, G. Hautier, W. Chen, W. D. Richards, S. Dacek, S. Cholia, D. Gunter, D. Skinner, G. Ceder, and K. A. Persson, The Materials Project: A materials genome approach to accelerating materials innovation, APL Mater. **1**, 011002 (2013).

[29] V. Kopskỳ and D. Litvin, *International Tables for Crystallography*, Vol. E, *Subperiodic Groups* (Kluwer Academic Publishers, 2002).

[30] X. Chen, D. Wang, L. Li, and B. Sanyal, Giant spin-splitting and tunable spin-momentum locked transport in room temperature collinear antiferromagnetic semimetallic CrO monolayer, Appl. Phys. Lett. **123**, 022402 (2023).

[31] P.-J. Guo, Z.-X. Liu, and Z.-Y. Lu, Quantum anomalous hall effect in collinear antiferromagnetism, npj Comput. Mater. **9**, 70 (2023).

[32] M. I. Aroyo, *International Tables for Crystallography*, Vol. A, *Space-Group Symmetry* (Springer, 2016).

[33] D. B. Litvin and T. R. Wike, *Character Tables and Compatibility Relations of the Eighty Layer Groups and Seventeen Plane Groups* (Plenum Publishing Corporation, 2012).

[34] G. Kresse and J. Furthmüller, Efficiency of *ab-initio* total energy calculations for metals and semiconductors using a plane-wave basis set, Comput. Mater. Sci. **6**, 15 (1996).

[35] G. Kresse and J. Furthmüller, Efficient iterative schemes for *ab initio* total-energy calculations using a plane-wave basis set, Phys. Rev. B **54**, 11169 (1996).

[36] G. Kresse and D. Joubert, From ultrasoft pseudopotentials to the projector augmented-wave method, Phys. Rev. B **59**, 1758 (1999).

[37] J. P. Perdew, K. Burke, and M. Ernzerhof, Generalized gradient approximation made simple, Phys. Rev. Lett. **77**, 3865 (1996).

[38] S. L. Dudarev, G. A. Botton, S. Y. Savrasov, C. J. Humphreys, and A. P. Sutton, Electron-energy-loss spectra and the structural stability of nickel oxide: An LSDA+U study, Phys. Rev. B **57**, 1505 (1998).